Channel Scalability of Silicon Nitride (De-)multiplexers for Optical Interconnects at 1 μm

Citation for the original published paper (version of record):

Caut, A., Girardi, M., Torres Company, V. et al (2024). Channel Scalability of Silicon Nitride (De-)multiplexers for Optical Interconnects at 1 μm. Journal of Lightwave Technology, 42(1): 276-286. http://dx.doi.org/10.1109/JLT.2023.3306478

(article starts on next page)

Channel Scalability of Silicon Nitride (De-)multiplexers for Optical Interconnects at 1 μm

Alexander Caut, Marcello Girardi, Victor Torres-Company, *Senior Member Optica*
Anders Larsson, *Fellow Optica, Fellow IEEE* and Magnus Karlsson, *Fellow Optica, Fellow IEEE*
Photonics Laboratory, Department of Microtechnology and Nanoscience, Chalmers University of Technology, SE-412 96 Göteborg, Sweden

***Abstract*—This paper presents an investigation of the channel scalability of silicon nitride (Si_3N_4)-based (de-)multiplexers in the 1-µm band (1015-1055 nm). We discuss 4-, 8- and 16-channel demultiplexers based on arrayed waveguide gratings (AWGs) and cascaded Mach-Zehnder interferometers (MZIs), with corresponding channel spacings of 8, 4 and 2 nm. Gaussian and flat-top response devices are considered for both technologies and we analyze the insertion loss, temperature sensitivity, response flatness, footprint and crosstalk (XT). We study the impact of the number of channels on the insertion loss and XT level. In the experimental part, we demonstrate a 4-channel Gaussian AWG. We also demonstrate 4-channel Gaussian and flat-top cascaded MZIs, based on multimode interferometers (MMIs) and directional couplers (DCs). The AWG is attractive due to its small footprint but its high manufacturing complexity makes the device more prone to fabrication defects, which can lead to higher loss and higher XT. For the Gaussian AWG and MZI, the XT level is approximately the same and increases with the number of channels from -28 to -23 dB at 4 and 16 channels respectively. The flat-top MZI has no extra-loss with respect to the flat-top AWG and has a better tolerance to high temperature operations. However, due to wavelength sensitive DCs, the XT of the flat-top MZI is higher than that of the flat-top AWG except for a 16-channel system.**

***Index Terms*—Optical interconnects, silicon nitride, arrayed waveguide grating, Mach-Zehnder interferometer, multimode interferometer, channel spacing, insertion loss, crosstalk, manufacturing tolerance.**

I. Introduction

In the past years, global data traffic has been substantially growing, pushing the current interconnects in data centers further to their limits. With the cloud services becoming strongly popular, future hyperscale data centers will require new architectures based on short-reach optical interconnects with a capacity of several Tb/s [1], [2] while keeping costs and energy consumption low [3], [4]. Short-range interconnects are dominant in data centers and occupy 95% of all links [5]. These links use the combination of GaAs-based vertical-cavity surface-emitting lasers (VCSELs) and OM4 multimode fibers (MMFs) at 850 nm [2], [6], [7]. This solution is cost effective and reduces the power consumption. However, the length of these links is limited by the chromatic and modal dispersion at high data rates and high propagation loss [7], [8]. Therefore, longer-reach interconnects (between 0.3 and 10 km) use combinations of 1310 nm InP-based distributed feedback laser sources and single-mode fibers (SMFs) [2], [7]. As these longer links are far less dominant compared to short ones, both cost and capacity are more problematic than power consumption. This InP-based technology is also compatible with Si-platforms and the dispersion and attenuation are far less significant at this wavelength. However, it remains less cost effective than GaAs-based VCSELs and more difficult to fabricate [2], [7]. A more cost-efficient alternative for longer links would be the use of recently developed GaAs VCSELs operating at 1060 nm [7], [9]. Moreover, the combination with SMFs would allow a good reduction in dispersion and propagation losses compared to interconnects operating at 850 nm [2], [8], [10]. To further extend the wavelength of VCSELs towards 1310 nm or even 1550 nm, InP compounds would be required, but the devices would suffer from higher threshold currents [11]. Thus, the 1060 nm GaAs VCSELs were selected to face the challenge of building high bandwidth density optical interconnects with capacities of several Tb/s. Due to the limited modulation bandwidth of these VCSELs (30 GHz) [1], the use of wavelength division multiplexing (WDM) would be required to meet the targeted link capacity.

Si_3N_4 technology is being used since it is transparent in the 1-µm band and presents good tradeoffs between device's footprint, fabrication tolerance, propagation losses and phase errors [10], [12], [13]. On one hand, a SiN platform designed in the 1-µm band was demonstrated in our previous work and proposed a package of inverse tapers, ring resonators, arrayed waveguide gratings (AWGs), cascaded multimode interferometers (MMIs) and single Mach-Zehnder interferometers (MZIs) [2]. In that case, the designed channel spacing of the AWG was 8 nm. On the other hand, HPE labs demonstrated SiN-based demultiplexers for 990-1065 nm with channel spacing of 25 nm [10]. Their study focused on 4-channels AWGs and cascaded MZIs and compared their insertion loss, crosstalk, signal flatness, footprint, thermal response and channel accuracy. Their 4-channel Gaussian and flat-top AWGs had respective insertion losses of 0-1 dB and 2-4 dB. In addition, their 1 x 4 flat-top lattice MZI filters could operate, alongside their flat-top AWGs, at temperatures as high as 80 °C without requiring thermal tuning.

Here, our envisioned 1 μm optical interconnect consists of multi-wavelength VCSEL arrays flipped chipped over a Si_3N_4 platform and co-packaged Coarse WDMs (CWDM) as shown in Figure 1 [2]. Due to the limited VCSEL's gain bandwidth, the channel spacing needs to be reduced [9] and is set to 8 nm for a 4-channel system. The 4-wavelength VCSEL arrays (wavelengths located at 1023, 1031, 1039 and 1047 nm) are

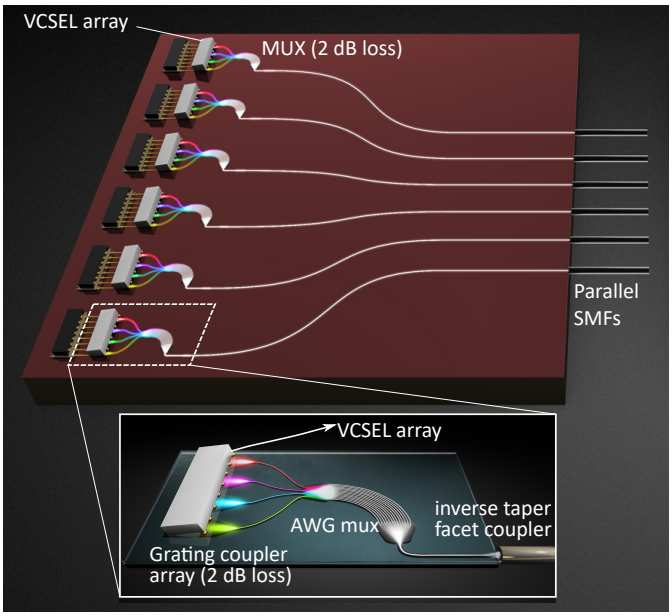

Fig. 1. Integrated transmitter that includes VCSEL arrays flip-chipped over grating couplers and multiplexing devices (MUX) [2], which are in focus of this work.

flip-chipped over the Si_3N_4 platform in which the wavelengths are then multiplexed. The (de-)multiplexers in our platform need to be fabrication tolerant, demonstrate low insertion loss and low crosstalk level. They also need to tolerate possible wavelength shifts from the flip-chipped VCSELs due to fabrication or temperature variations. Hence, we first considered AWGs due to their compact size, low insertion loss and low crosstalk [10]. Moreover, they are easier to manufacture than other types of demultiplexers such as reflective AWGs [14], [15] or echelle diffraction gratings [14], [16]. Alternatively, cascaded MZIs are easy to fabricate and can provide low insertion loss [17], [18] and crosstalk level below -20 dB with stage doubling [10] and wavelength insensitive power splitters [18]. To tolerate wavelength shifts of the lasers, a flat-top response demultiplexer is generally preferred to ordinary Gaussian response devices [10], [19]. Hence, flat-top designs were included into the fabrication run. The design parameters and desired performances are summarized in table I. We demonstrate 4-channel Gaussian AWG, Gaussian and flat-top cascaded MZIs with 8 nm channel spacing. The cascaded MZIs in this work, with respect to the MZI lattice filter designs of HPE labs based on directional couplers (DCs), mostly use MMIs as power splitters. Moreover, our flat-top cascaded MZIs use a combination of MMIs and DCs. We also provide a complete analysis of the crosstalk XT of these demultiplexers with 4 channels and we then extrapolate via simulations the study to 8 and 16 channels. Since the VCSELs are manufactured in the same array and have a limited gain bandwidth [9], the channel spacing has to be reduced for multi-channel systems: 4 nm for 8 channels and 2 nm for 16 channels.

This paper is organized as follows: Section II presents an analysis of manufactured 4-channel AWGs and cascaded MZIs with 8 nm spacing in terms of simulated transmission, sensitivity to temperature and manufacturing tolerances. In section III, we extrapolate, via simulations, the study of these (de-)multiplexers to more (8 and 16) channels. In this paper, we compare the manufacturing tolerance in terms of channel allocation when the dimensions (width and thickness) and refractive index of the waveguide vary and the manufacturing complexity. We also compare the simulated average insertion loss and crosstalk with the number of channels. The Gaussian and flat-top devices are also compared and we determine which device is most promising in future WDM interconnects.

TABLE I
LIST OF TARGET SPECIFICATIONS FOR THE MUX/DEMULTIPLEXING COMPONENTS.

Design parameters	Value
Channel spacing	8 nm
Channel optical 3 dB-bandwidth	3 nm
Number of channels	4
Wavelength accuracy	2 nm
Throughput loss	2 dB
Crosstalk	-20 dB

II. Design and fabrication of 4-channel AWGs and MZIs

Our photonic integrated circuit (PIC) needs to achieve both low propagation loss while having a small footprint. The use of thick square-shaped Si_3N_4 waveguide would allow a strong mode confinement and bending radii close to 10 μm. In addition, it was found that thick single mode waveguides can reduce the effective index variation by a factor of 6 [10] and thus leading to more robust devices to fabrication deviations. However, thick single mode waveguides also suffer from higher sensitivity to sidewall roughness, increasing scattering losses which can reach up to 30 dB/m [20]. In contrast to this, low propagation loss can be achieved with ultra-thin waveguides, but at the cost of large bending radii and increased device footprint [2], [21], not to mention our full PIC includes grating couplers, which are more efficient with thick waveguides. We settled on a waveguide cross-section geometry of 900 x 160 nm (width x height) to realize small footprint devices with sufficiently low insertion losses. The Si_3N_4 waveguide is sandwiched between a 3-µm thick SiO_2 substrate and a 3-µm thick SiO_2 cladding. The refractive indices of Si_3N_4 and low-pressure chemical vapor deposition (LPCVD) SiO_2 are measured with ellipsometry and are, respectively, 2.004 and 1.4485 at a wavelength of 1035 nm. These values were used for all our simulations. In the experimental section we will next describe the characterization results of AWGs and cascaded MZIs as 4-channel demultiplexing devices. In our previous work, a Gaussian 4 x 4 AWG and a single 2 x 2 MZI [2] were demonstrated. The AWG and the MZI had respective footprint of 1000 μm x 1000 μm (excluding the input and output waveguides) and 1600 μm x 820 μm. The insertion loss was within 2 dB and the crosstalk of the AWG around -16 dB. In this section, we reduced the footprint of both demultiplexers while conserving the overall performance. In addition, Gaussian and flat-top 1 x 4 MZI demultiplexers are demonstrated.

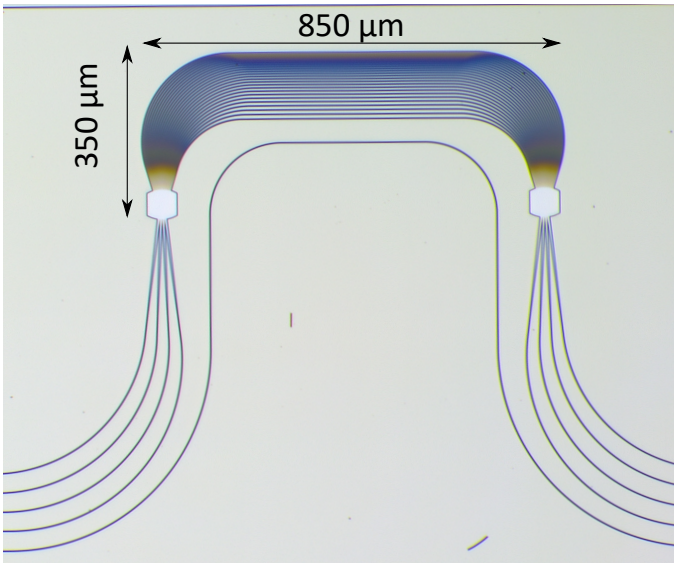

Fig. 2. Manufactured AWG with the reference waveguide.

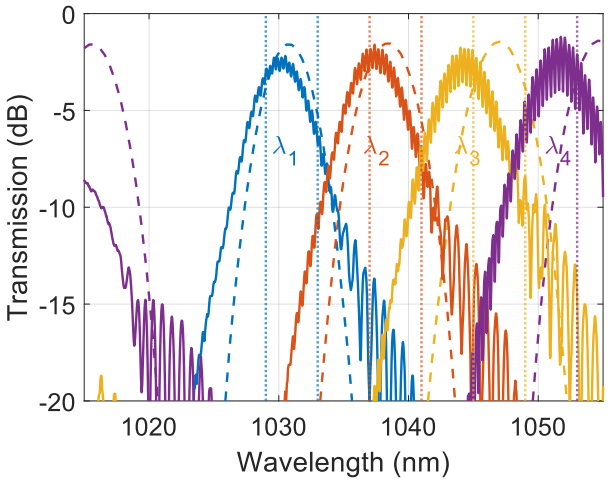

Fig. 3. Measurement and simulation of the manufactured Gaussian AWG. The solid lines correspond to the measurements and the dashed lines indicate the simulated transmission from the same input waveguide. The vertical dotted lines represent the VCSEL passband wavelength accuracy for each channel, centered around the target wavelength.

TABLE II
LIST OF PARAMETERS OF THE AWG.

Design parameters	Value (μm)
FPR length	62.7
Length increment	15.42
Receiver waveguide separation	5
Receiver taper width	4.6
Receiver taper length	200
Array waveguide separation	1.5
Array taper width	1.2
Array taper length	40
Minimum bending radius	150

A. Designed AWG

The AWG is a popular device for wavelength division multiplexing due to its small size, low crosstalk level and fabrication tolerance [10]. It mainly consists of input/output waveguides and two free propagation regions (FPRs) connected by a set of arrayed waveguides. The adjacent arrayed waveguides have a path length difference that determines the center wavelength and channel spacing. In table II are presented the values of the main design parameters for a 160 nm-thick SiN platform. To minimize the insertion loss and to maximize the channel bandwidth, the input and arrayed waveguides are tapered near the FPR section. The gap between the input waveguides is 400 nm and is 300 nm for the arrayed waveguides near the FPR. The device has an overall footprint of 850 μm x 350 μm without the input and output waveguides, which is 3.4 times smaller than the device in [2].

We evaluated the AWGs in terms of signal flatness, bandwidth, insertion loss and crosstalk. The VCSEL's resonance wavelength depends on the etch depth into the current injection layer and it was found that the wavelength shifts by 0.95 nm per 1 nm of etching [9]. We assumed then that the target resonance wavelength can be hit with an accuracy of ±2 nm [22].

The simulations were carried out with 2D Beam Propagation Method (BPM) and the designed free spectral range (FSR) for the AWG is 40 nm. Figure 2 shows the manufactured AWG designs and Figure 3 illustrates the measured transmission of a Gaussian AWG using the first input waveguide from the bottom. The simulation is plotted on the same graph for comparison. The measured transmission is normalized to the coupling loss between the lensed fibers to the chip, and normalized relative to a reference waveguide manufactured close to the device (Figure 2), which will determine the device's insertion loss. We define the insertion loss as the device's throughput loss excluding fiber-chip coupling and waveguide propagation loss. The fiber-to-fiber loss for the reference waveguide is about 10 dB. The AWG achieves an average insertion loss of -1.83 dB per channel. The device also presents strong oscillations possibly due to random phase errors in the array section and to back reflections between the waveguides and the lensed fibers. In addition, for a spectral shift of 2 nm from the VCSELs, the measured average transmission decrease is 2.3 dB, which is 1.1 dB less than the value predicted by the simulations. The crosstalk XT is defined as the difference between the peak level of the wavelength channel and of an undesired peak level coming from another channel, which will be discussed in more details in Section III of the paper as it will be a limiting factor mainly in the receiver.

B. Designed cascaded MZIs

Cascaded MZIs represent a low loss alternative to AWGs to realizing CWDM devices. 1 × 4 SiN-cascaded MZIs based on MMIs were reported in the O-band [23], [24], [25] and DC-based SiN-cascaded MZIs in the 1-μm wavelength range [10] with a demonstrated channel spacing of 25 nm.

The proposed designs in this paper include MMI-based devices for Gaussian response demultiplexers and hybrid MMI/DC-based devices for flat-top response demultiplexers that are more tolerant to wavelength changes. The Gaussian

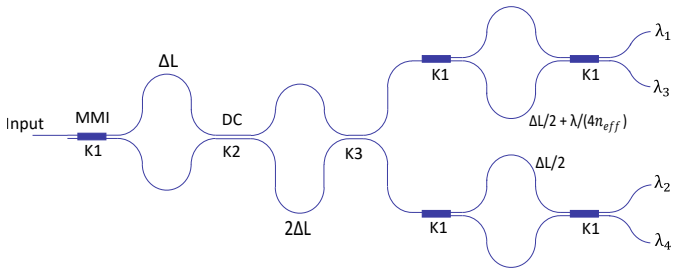

Fig. 4. Design of the flat-top cascaded MZI. The first stage separates the odd from the even wavelengths with a FSR of 16 nm and the second separates the two sets of wavelength with a FSR of 32 nm. Here, K1 = 0.5, K2 = 0.29, K3 = 0.08, λ = 1.035 μm and ΔL = 35.76 (or 35.06) μm. n_{eff} = 1.56 is the mode effective index.

TABLE III
LIST OF PARAMETERS OF THE CASCADED MZIS.

Design parameters	Value (μm)
MMI slab-section length	70
MMI taper width	1.7
MMI taper length	20
DC K = 0.29 length	34
DC K = 0.29 gap	0.44
DC K = 0.08 length	13
DC K = 0.08 gap	0.44
Length increment	35.76
Minimum bending radius	50

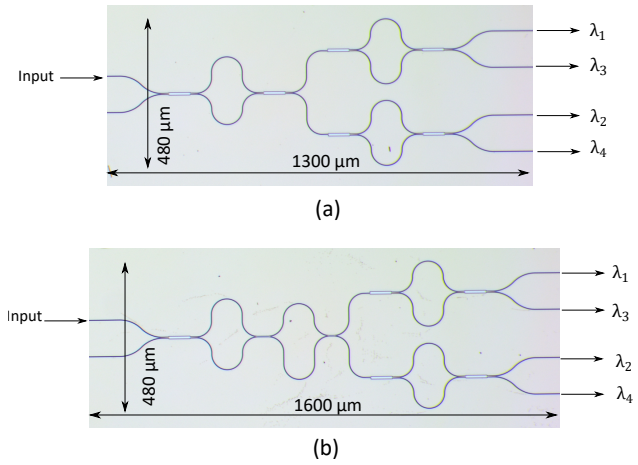

Fig. 5. Manufactured (a) Gaussian cascaded MZIs based on MMIs and (b) flat-top cascaded MZIs based on MMIs and DCs.

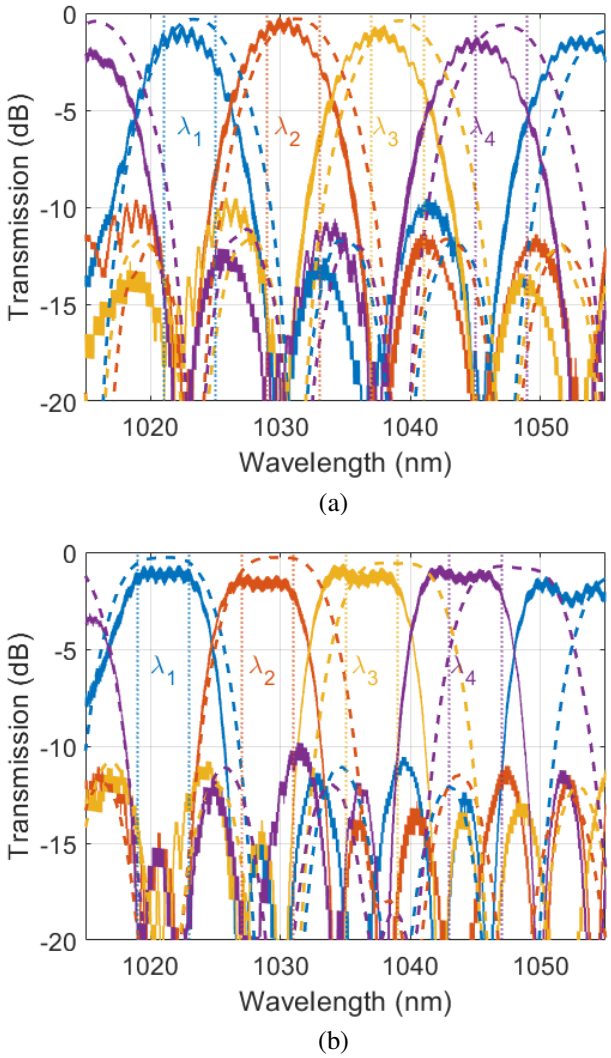

Fig. 6. Measurements and simulations of the (a) Gaussian MZI filter and (b) flat-top filter. The solid lines correspond to the measurements and the dashed lines indicate the simulated transmission of the devices. The vertical dotted lines represent the VCSEL passband wavelength accuracy for each channel, centered around the target wavelength.

cascaded MZIs only require 3 dB power splitters (corresponding to a cross-coupling coefficient K = 0.5) and 1st order filters on each stage. However, flat-top devices require at least a second order filter on the first stage and a more careful approach regarding the design of the power splitters. Indeed, to flatten the MZI's response without introducing extra insertion loss, power splitters with arbitrary coefficients will be required [10], [13], [18]. Therefore, we considered two kinds of power splitters for our device: the DC and the MMI. DCs are of interest because arbitrary cross-coupling coefficients can be easily obtained [10]. For design and fabrication simplicity, the DCs in this paper are straight. The only drawback of conventional DCs is the fact that they are wavelength sensitive, which could lead to higher crosstalk [10], [18]. This is why the MMI option was also explored, as it is much less sensitive to wavelength changes than straight DCs and more fabrication tolerant [2], [26]. However, arbitrary cross coupling coefficient MMIs are more difficult to obtain and can introduce additional losses [18]. Therefore, for our MZI devices, MMIs are used for cross coupling coefficient K = 0.5 and DCs for K = 0.29 and 0.08. To reduce the insertion loss, the MMIs are equipped with linear tapers. Table III shows the main design parameter of the manufactured cascaded MZIs. We restricted ourselves to 2 x 2 MMIs as it was found in our previous research that our 1 x 2 MMI design for this SiN platform had a slightly higher loss than the 2 x 2 design [2].

In Figure 5 we show the two fabricated cascaded MZI filters. In the fabrication run were also included devices with slightly different base length differences to study the impact on the transmission spectrum. The Gaussian and flat-top devices

have a base length difference of, respectively, 35.76 μm and 35.06 μm. This resulted in a small spectral shift of -1.5 nm for the flat-top device. The Gaussian and flat-top devices have respective footprints of 1300 μm x 480 μm and 1600 μm x 480 μm. In our previous work, the bending radius of the interference arms of the MZI was 200 μm to avoid radiation losses in the bent waveguides [2]. This dimension was decreased down to 50 μm to reduce the size of the devices. Therefore, the proposed 1 x 4 demultiplexers using MZI filters can fit within the 1 x 2 MZI in Ref [2]. The characterization and simulation results are shown in Figure 6. The simulations were carried out with 2.5D-FDTD (varFDTD) and each stage of the demultiplexer was simulated separately for fast and accurate results. The Gaussian and flat-top devices achieve insertion losses of 0.6 and 1.1 dB respectively, which indicates that the reduced bending radius of the interference arms does not penalize the overall performance of the device. It can be observed that in addition to offering a larger bandwidth, the flat-top MZI reduces the bandwidth of the side-lobes. However, random side-lobes occur at the center of some channels with respect to the Gaussian device. Effective index variations due to small dimension variations of the waveguide can lead to phase errors, which can translate into higher crosstalk level [10]. In addition, the channel spacing is 7.6 nm ± 0.4 nm. Phase shifters could be introduced in our future cascaded MZIs to make them more robust to fabrication deviations [27]. The deviations in the channel spacing relative to the simulations are possibly due to inaccurate refractive indices used in the design and can be accommodated in future fabrication runs.

Finally, one can notice that the flat-top device offers a significant signal flatness compared to the Gaussian MZI filters. Indeed, from the characterization results in Figure 6, a VCSEL spectral shift of 2 nm would lead to an average transmission decrease per channel of 0.9 dB for the Gaussian device and 0.3 dB for the flat-top filter.

C. Sensitivity to temperature

The thermal sensitivities of the two demultiplexing technologies are compared in this section. Indeed, the VCSELs need to operate at temperature reaching at least 60°C and have a temperature sensitivity of 75 pm/°C [9]. Therefore, to reduce power consumption with avoiding electrical tuning, the pass-band wavelengths of the AWG and of the cascaded MZIs have to be sufficiently large in order to suit the VCSEL's spectral shift at high temperature. Here, we simulate the thermal response of both demultiplexing technologies. The thermo-optical coefficients for silicon nitride and silica are 2.5×10^{-5} /°C and 0.96×10^{-5} /°C respectively [28], [29]. The refractive indices of these materials at 60°C was deduced and then incorporated in our simulations. The array section of the AWG is entirely covered by the thermal heater, but for the cascaded MZI, we only heat the bent waveguides of the second stage. In Figure 7 are plotted the simulated thermal responses of a flat-top AWG and of a flat-top cascaded MZI. It was found that the spectral shifts are 14.3 pm/°C for the AWG and 7.7 pm/°C for the MZI, which are values close to

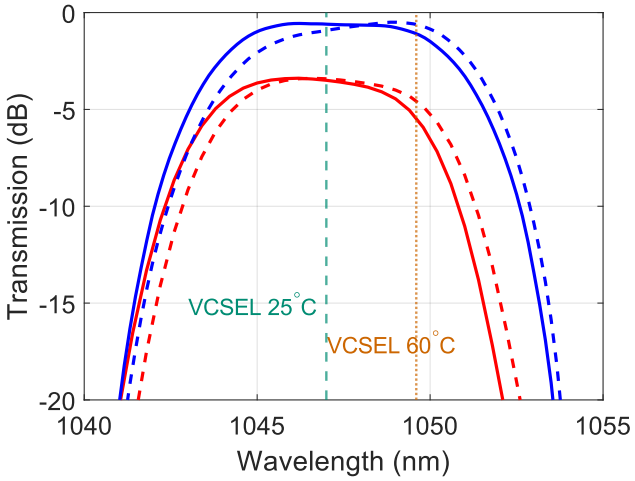

Fig. 7. Simulated thermal response of one channel of the AWG (red curves) and of the cascaded MZI (blue curves). The continuous and dashed curves correspond to ambient temperature (25°C) and to 60°C respectively.

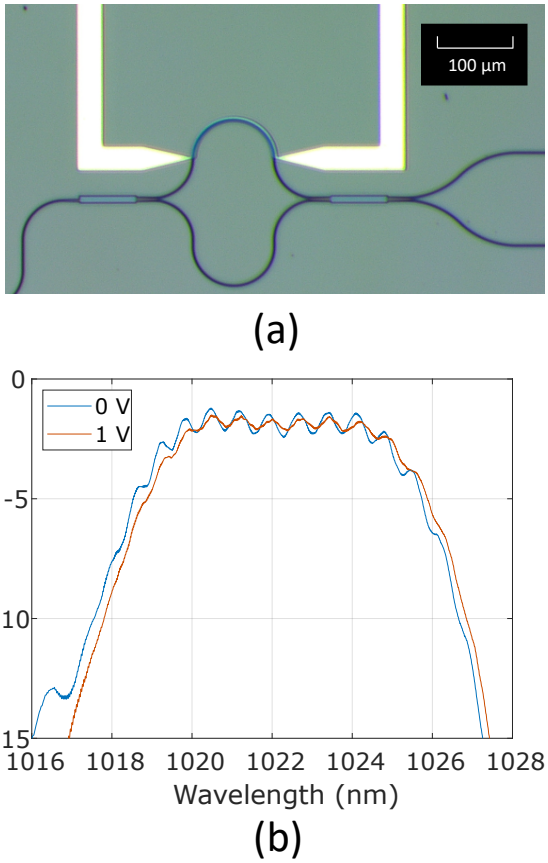

Fig. 8. Electrical tuning of one channel of a flat-top cascaded MZIs: (a) Microscope image of the upper arm of the device with a Pt thermal heater. (b) Measurements of one channel when tuning the applied voltage on the device.

the results in Ref [10]. The VCSEL's spectral shift is also plotted for comparison. We can observe from the figure that the AWG presents a power penalty of 1.1 dB at 60 °C, which is significant compared to that of the MZI (0 dB). We can deduce from Figure 7 that the AWG is more sensitive than

the cascaded MZI to high temperature variations and that the bandwidth of the designed flat-top cascaded MZI is large enough to operate at high temperatures without any power penalties. The electrical tuning of a flat-top cascaded MZI was also measured as shown in Figure 8. The second stage of the device was equipped with 200 nm-thick Platinum thermal heaters and a DC voltage was applied with electrical probes to measure the wavelength shift of the device. The measurements show the channel's response for an applied voltage up to 1 V and the measured wavelength shift of the device was 0.3 nm/V. Any voltage higher than 2 V resulted in a significant loss penalty and a channel bandwidth reduction. The applied voltage would result in a temperature of approximately 65°C according to our simulations (or +40°C/V). A thermal camera would allow for a more precise estimation of the temperature, but we had no access to that at the time of characterization.

D. Manufacturing tolerance and channel accuracy

In this section, we study the manufacturing tolerance of the AWG and of the cascaded MZI. We simulate the position of the center wavelength $\Delta\lambda$ when the waveguide width and thickness deviate from the target values which are 900 nm and 160 nm respectively (Figure 9 (a) and (b)). The simulations were performed with a step of 5 nm in width and 2.5 nm in thickness. The results in Figure 9 (a) and (b) reveal that the waveguide thickness has a larger impact on the center wavelength position than the width. The wavelength shift due to waveguide thickness and width variation are denoted $\Delta\lambda$/dt and $\Delta\lambda$/dw respectively. The calculated average wavelength shift in thickness variation is $\Delta\lambda$/dt = 0.98 nm/nm for the AWG and 0.79 nm/nm for the cascaded MZIs. The wavelength shift in width variation is $\Delta\lambda$/dw = 0.13 nm/nm for the AWG and 0.07 nm/nm for the MZI. Since the devices are based on thin waveguides, the effective index of the propagating mode will be more dependent on thickness variations than on width variations [10], which explains the strong wavelength shift with the thickness in Figure 9 (a) and (b). The found results are of same magnitude order than the results in Ref. [10]. The thickness variation of our wafer was around ±2.5 nm from the targeted thickness, which would result in a spectral shift of 0.32 nm for the AWG and 0.19 nm for the MZI in both directions. In addition, such thickness variation leads to an effective index shift dn_{eff} of $\pm 3.1*10^{-3}$, which could result in an increase of the crosstalk level for the AWG [10]. We also studied the impact of calibration error of the ellipsometer, that could potentially lead to a shift between the real refractive index and the one used in the design. Therefore, simulations were also realized when the waveguide index varies from the expected value (Figure 9 (c)). At a wavelength of 1035 nm, we measured an index of 2.004 for LPCVD Si_3N_4 with the ellipsometry method. An increase of 0.2 % of the waveguide's refractive index leads to a value of 2.008. The calculated wavelength shift in the Si_3N_4 waveguide is 1.8 nm for the AWG and 1.2 nm for the cascaded MZIs, thus proving the AWG to be more sensitive than the MZI to tool calibration error.

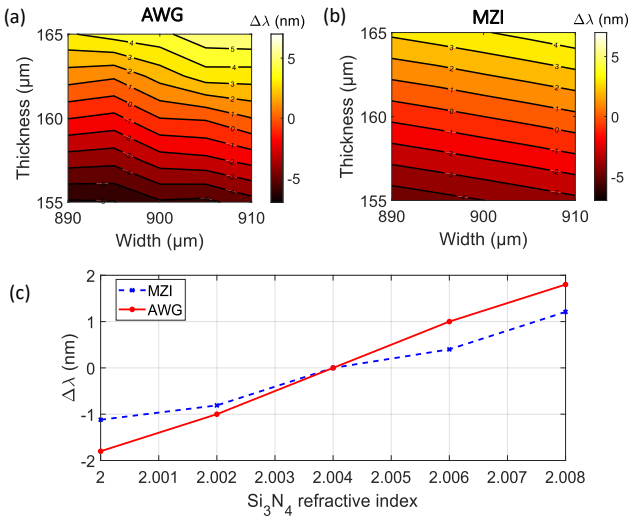

Fig. 9. Simulations of the channel accuracy with the waveguide thickness and width variations for the AWG (a) and the MZI filter (b). $\Delta\lambda$ = 0 when the center wavelength (1035 nm) is hit. (c) Simulation of the central wavelength with the refractive index of the Si_3N_4 waveguide.

E. Discussion

In table IV are summarized the results from the simulations and characterizations (written in parenthesis) for AWGs and cascaded MZIs. It includes the insertion loss (IL), the power decay when the VCSEL spectrum shifts by 2 nm in one direction (ΔIL_{2nmm}), robustness to temperature ($\Delta\lambda/\Delta T$) and to waveguide geometry deviations ($\Delta\lambda/\Delta t$ and $\Delta\lambda/\Delta w$).

TABLE IV
SUMMARIZED RESULTS FROM SIMULATIONS AND MEASUREMENTS OF THE 4-CHANNEL DEVICES.

	Gaus. AWG	Flat AWG	Gaus. MZI	Flat MZI
IL (dB)	1.54 (1.83)	3 (..)	0.4 (0.6)	0.5 (1.1)
Size (mm^2)	0.28	0.28	0.57	0.66
ΔIL_{2nm} (dB)	3.4 (2.3)	1.8 (..)	0.8 (0.9)	0.2 (0.3)
$\Delta\lambda/\Delta T$ (pm/°C)	14.3	14.3	7.7	7.7
$\Delta\lambda/\Delta t$ (nm/nm)	0.98	0.98	0.79	0.79
$\Delta\lambda/\Delta w$ (nm/nm)	0.13	0.13	0.07	0.07

It can be noticed that the cascaded MZIs have lower insertion loss than the AWGs. In addition, the cascaded MZIs have a better tolerance to temperature and to waveguide dimension deviations. More fabrication tolerant demultiplexers could be obtained by widening the waveguide in the path length difference section [27], [30].

III. SCALABILITY TO 8 AND 16 CHANNELS

Flat-top cascaded MZIs have shown to be an attractive alternative to AWGs in a 4-channel CWDM. We also designed and simulated 8- and 16-channel CWDM devices to study the evolution of scalability, insertion loss and crosstalk. As already stated in Section I, since the VCSELs are manufactured in the same array and have a limited gain bandwidth [9], we need to reduce the channel spacing of the demultiplexers. Therefore, the channel spacing of the 8-channel demultiplexers is set to 4 nm and 2 nm for the 16-channel demultiplexers.

As we selected the option of a 4-channel VCSEL array for our integrated photonic circuit, the 8- and 16-channel devices were not manufactured.

A. Scalability: footprint and EBL writing

The footprint is a crucial factor, not only for fitting all the devices on one chip but in the fabrication workflow as well. Indeed, we pattern the devices with a serial process, i.e. electron beam lithography (EBL), where the device is divided in fields of 1x1mm^2. If the device is larger than the field, stitching errors might occur between fields, increasing the optical loss of the device. For this reason, a single AWG could minimize the number of fields needed, especially for a large number of channels, as showed in Figure 10. The size of the AWG is compared to that of the cascaded MZIs for different number of channels (4, 8 and 16). Since the channel spacing is reduced, the FSR is kept the same for both devices. On the one hand the base length difference of the AWGs will be the same as for 4 channels. However, the main changes on the designs are the length of the FPRs and the increased number of arrayed waveguides to ensure a uniform loss for all output channels. The sizes of the designed 4-, 8- and 16-channel AWGs are 0.28, 0.58 and 1.23 mm^2 respectively. On the other hand, the cascaded MZI filter is a 2^N-channel demultiplexer, (N being the number of stages) and the base length difference is doubled when increasing N: 75.37 and 150.37 μm for 8 and 16 channels respectively. Therefore, the corresponding sizes of the 4-, 8- and 16-channel Gaussian cascaded MZIs are 0.57, 2.05 and 5.7 mm^2. We can see in Figure 10 that cascaded MZIs device is twice the size of the AWG at 4 channels, and 5 times bigger at 16 channels.

However, the other factor to consider is the patterned area of the two types of devices. Since EBL is a serial process, the exposed area determines the writing time, thus the AWG reported in this work took on average seven times more to be exposed compared to the MZIs in 4-channel demultiplexing. This is less crucial for parallel processes, e.g., a UV lithography, however, the dense areas with small gaps (300 nm) near the FPR makes the AWG prone to fabrication defects. In these areas, the development of the resist is more challenging and resist residues can cause an improper etching, which leads to additional losses.

The results for both devices are plotted in Figure 11 and we can clearly see that the AWG's writing area becomes quickly problematic at 16 channels. Indeed, the AWG has a writing surface of almost 400000 μm^2 whereas the cascaded MZIs device has a surface of approximately 35000 μm^2 at 16 channels. The considerable writing surface value of the 16-channel AWG is due to the exceeding number of arrayed waveguides which reaches 128 and also due to the large FPRs. In contrast to this, the cascaded MZI consists of 15 filters with an EBL area of approximately 1700 μm^2 each and of a few waveguides which are hundreds of microns long to make sure that the filters do not overlap with each other.

B. Scalability: insertion loss and crosstalk

In this section, we analyze the insertion loss and crosstalk with the number of channels for both technologies. The

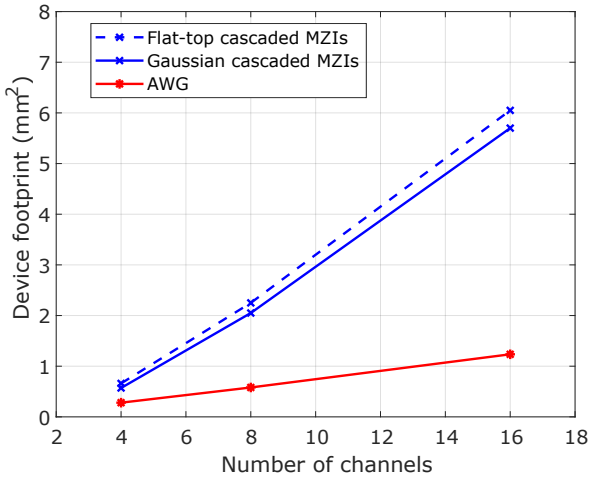

Fig. 10. Footprint of the AWG and of the cascaded MZIs with the number of channels.

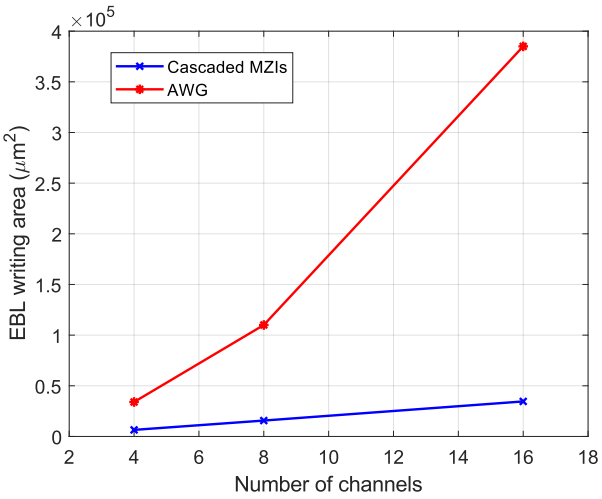

Fig. 11. EBL writing area of the AWG and of the cascaded MZIs with the number of channels.

transmissions of the 8- and 16-channel devices are plotted in Figure 12. As for section II, the cascaded MZIs were simulated in blocks with varFDTD, each block corresponding to a single MZI while the BPM method was used to simulate the AWGs. Indeed, the BPM simulation technique was already used in our previous work on a 4-channel AWG at 1 μm [2] and the measured insertion loss, channel spacing, and channel bandwidth were in good agreement with the simulations. Therefore, the BPM method was appropriate for the 8- and 16-channel AWGs.

To flatten the spectral response of our AWGs, parabolic MMIs are used at the input FPR of the AWG [19]. The flat-top AWGs have a lower transmission per channel than the cascaded MZIs, reaching almost -5 dB for 16 channels. However, the Gaussian AWG's spectrum is constant at -2 dB in average and the cascaded MZIs have a transmission between -1 and -0.5 dB. The crosstalk level, being a critical parameter, requires a deeper analysis for both devices when increasing the number of channels. When all the wavelengths

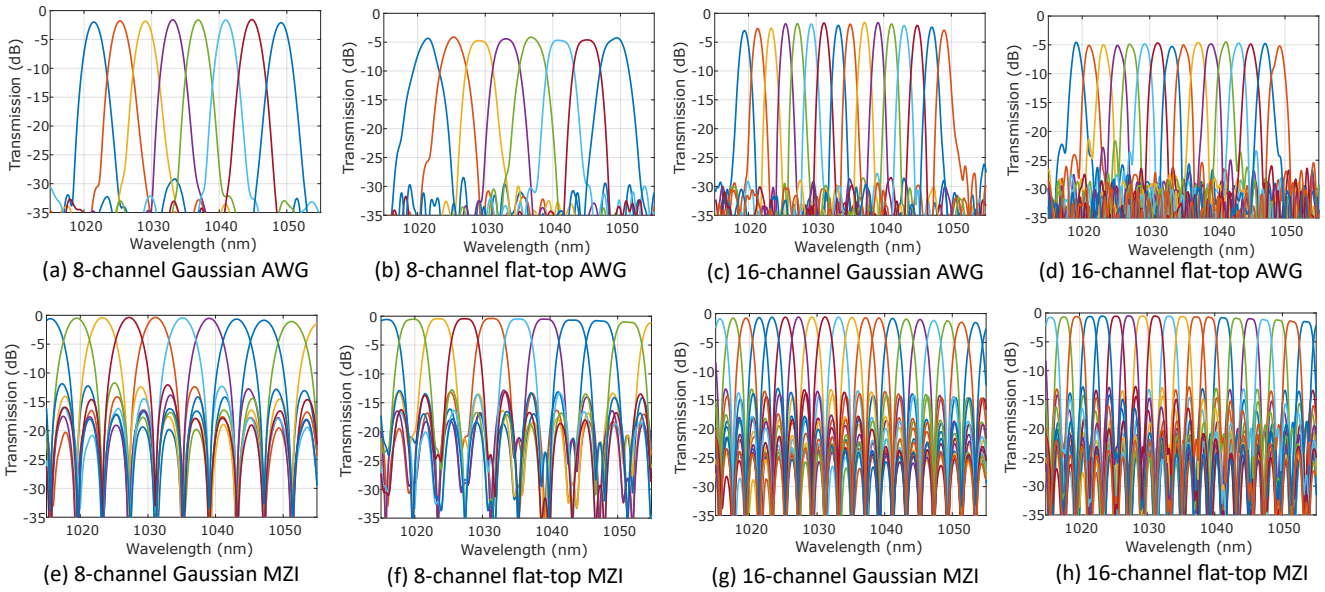

Fig. 12. Simulated transmissions of 8- and 16-channel AWGs and cascaded MZIs. The FSR is the same as for the 4-channel devices: 40 nm for the AWGs and 32 nm for the cascaded MZIs.

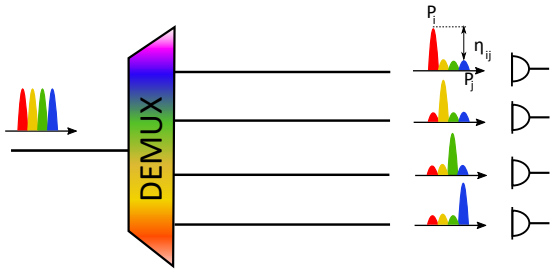

Fig. 13. Demultiplexer with photodetectors at the output channels. η_{ij} denotes the ratio P_j/P_i. P_i being the power of channel i and P_j the detected power from the channels j ($\neq$ i) contributing to higher crosstalk level.

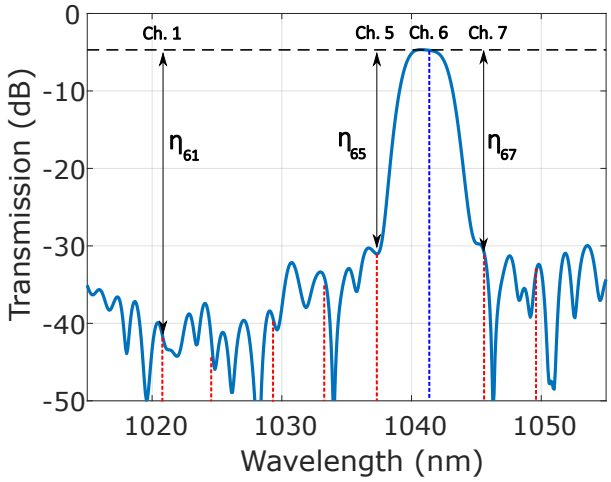

Fig. 14. Definition of the crosstalk with the example of the 8-channel flat-top AWG. Only channel No. 6 is plotted. The blue-dashed line corresponds to the signal from the VCSEL aligned with channel No. 6 and the red dashed lines correspond to the overlapping signals coming from the other VCSELs.

are demultiplexed, each channel will detect some undesired weak signals coming from the other, imperfectly attenuated, wavelengths. The sum of these signals from all the unwanted wavelengths will be defined as the total crosstalk XT_i received by the photodetector for channel i (Figure 13). The goal of this study is then to also determine if the number of channels will have a strong influence on the total received crosstalk XT_i.

Figure 13 illustrates a demultiplexing device with the wavelength separation and the detection of crosstalk in the photodetectors. In Figure 14 is shown an example response from one channel of an AWG with the corresponding crosstalks coming from the other channels. With I_i and R being respectively the photodiode current and responsivity, we have following expression for the detected current

$$I_i = R\left(P_i + \sum_{j\neq i} \eta_{ij} P_i\right) = RP_i\left(1 + XT_i\right), \qquad (1)$$

where η_{ij} denotes the ratio P_j/P_i and P_i is the power of channel i and P_j the detected power from the channels j ($\neq$ i), see Figure 13. Then, for the average received signal power for channel i is

$$< I_i^2 >= R^2P_i^2 + 2R^2P_i^2XT_i + R^2P_i^2(XT_i)^2 + \sigma_T^2, \qquad (2)$$

where σ_T^2 is the photodiode thermal noise variance which is the dominant noise source in these systems. If the crosstalk XT_i is small, then we can derive from equation (2) the signal-to-noise ratio for channel i (SNR_i) as

$$SNR_i = \frac{R^2P_i^2}{2R^2P_i^2XT_i + \sigma_T^2}, \qquad (3)$$

which can be rewritten as

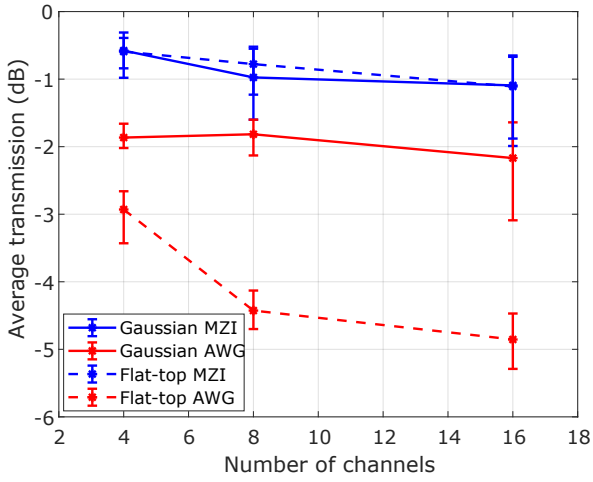

Fig. 15. Average transmission plotted with the number of WDM channels. Each circle corresponds to the average value and each error bar to the minimum and maximum simulated values.

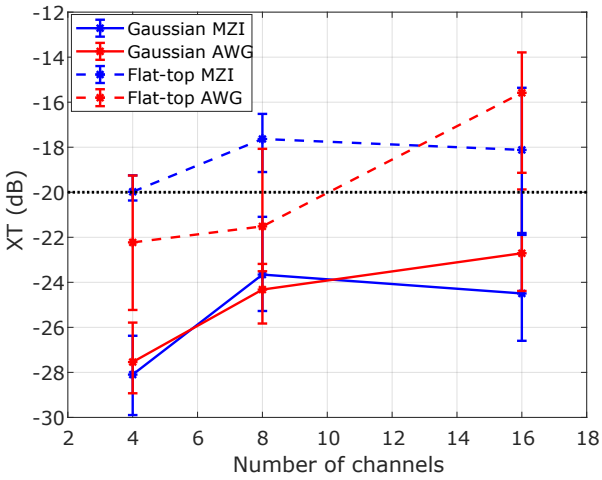

Fig. 16. Average crosstalk (XT) plotted with the number of WDM channels. Each circle corresponds to the average value and each error bar to the minimum and maximum simulated values. The horizontal dashed line corresponds to the maximum acceptable crosstalk level.

$$\mathrm{SNR}_i^{-1} = \frac{\sigma_T^2}{R^2 P_i^2} + 2\mathrm{XT}_i, \tag{4}$$

to highlight the impact of the crosstalk. Finally, we define the average received crosstalk as

$$\mathrm{XT} = \frac{1}{N}\sum_i \mathrm{XT}_i, \tag{5}$$

where N is the number of channels of the demultiplexer.

The crosstalk is then calculated using these equations for all devices. We select an acceptable total crosstalk level XT_i of -20 dB, although in a real system it will depend on the noise, signal power, data rates and many other parameters.

The results from these simulations are shown in Figures 15 and 16. It can be noticed in Figure 15 that the average transmission decreases with the number of channels as the device increases in size. The reason the loss increases with the number of channels for the cascaded MZIs is the increasing number of filters (and of power splitters, also source of additional loss). The simulations show that in overall, the total crosstalk slightly increases with the number of channels. The cascaded MZIs have a transmission ranging from -1 to -0.5 dB whereas the AWGs have a transmission close to -2 dB for a Gaussian device and between -3 and -5 dB for a flat-top device. The AWG has an XT level below -20 dB in every case except for the 16-channel flat-top AWG which has an XT level of -15.6 dB which is way above the target. Regarding the cascaded MZIs, the Gaussian MZIs have XT levels very similar to the Gaussian AWGs from 4 to 16 channels, ranging from -28 to -22 dB. However, the flat-top cascaded MZIs have crosstalk level slightly above -20 dB in every case, the minimum level being -19.9 dB for a 4-channel demultiplexer and the maximum -17.6 dB for a 8-channel device.

IV. Discussion and Tradeoffs

The insertion loss, the crosstalk and the device's footprint have been analyzed in the previous sections. We saw that in some cases, the AWG and the cascaded MZIs can both provide low XT level while maintaining low insertion loss for all channels. The other parameters to consider are the footprint and the EBL writing area. The latter factor determines the writing time and as shown in Figure 11 the AWG requires an EBL surface seven to eleven times more than the cascaded MZIs depending on the number of channels. In addition, the small gaps between the arrayed waveguides in the FPR section make the resist development more challenging and can lead to higher losses and crosstalk level if resist residues are left. This is even more problematic at 16 channels since the designed AWG has 128 waveguides in the array section. The results are summarized in Table V for all channel systems. The green and red colored cells in the table indicate the best and worst results respectively.

In the case of a 4-channel demultiplexer, the AWG is half the size of the cascaded MZIs (Figure 10). However, the Gaussian cascaded MZI provides the best XT result with a measured average of -14.5 dB. The Gaussian AWG has the second best measured XT level (-13 dB) and the flat-top cascaded MZI has an XT of -10 dB (Table V). The characterization results also highlight that the cascaded MZIs' transmissions are more in agreement with simulations than for the Gaussian AWG, which presents more ripples, possibly coming from phase errors at the FPRs or array section. From all the manufactured devices presented, the Gaussian cascaded MZI provides the measured XT level that is closest to the desired level (-20 dB) and is by far, the simplest to fabricate. The flat-top cascaded MZI is more tolerant to VCSEL misalignment but due to its too high measured XT level, and additional filters might be required to lower the crosstalk [10], [18].

For the 8-channel demultiplexer, the Gaussian AWG offers the lowest XT level (-24.3 dB), the second best result comes from the Gaussian cascaded MZIs (-23.7 dB) and the 3rd from the flat-top AWG (-21.5 dB). However, the cascaded MZI

TABLE V
RESULTS OF THE 4-, 8- AND 16-CHANNELS DEVICES (MEASURED VALUES IN BRACKETS)

4 channels	Gaus. AWG	Flat AWG	Gaus. MZI	Flat MZI
IL (dB)	1.54 (1.83)	3 (..)	0.4 (0.6)	0.5 (1.1)
XT (dB)	-27.5 (-13)	-22.2 (..)	-28.1 (-14.5)	-19.9 (-10)
Size (mm^2)	0.28	0.28	0.57	0.66
EBL (μm^2)	$3.4*10^4$	$3.4*10^4$	$6.5*10^3$	$6.5*10^3$
8 channels	Gaus. AWG	Flat AWG	Gaus. MZI	Flat MZI
IL (dB)	1.7	4.4	1	0.8
XT (dB)	-24.3	-21.5	-23.7	-17.6
Size (mm^2)	0.58	0.58	2.05	2.25
EBL (μm^2)	$1.1*10^5$	$1.1*10^5$	$1.6*10^4$	$1.6*10^4$
16 channels	Gaus. AWG	Flat AWG	Gaus. MZI	Flat MZI
IL (dB)	2.1	4.8	1.1	1.1
XT (dB)	-22.7	-15.6	-24.4	-18.1
Size (mm^2)	1.24	1.24	5.7	6.05
EBL (μm^2)	$3.85*10^5$	$3.85*10^5$	$3.5*10^4$	$3.6*10^4$

becomes already four times as big as the AWGs as shown in Figure 10 (2 mm^2 vs 0.58 mm^2). In addition, the AWGs have lower XT level than the cascaded MZIs in Gaussian and flat-topped demultiplexing. The flat-top AWG offers a good trade-off between size, XT and signal flatness. However, its insertion loss is considerably high (4.4 dB) and the device is also harder to manufacture than the 3 others. The Gaussian cascaded MZI offers a large channel bandwidth, low insertion loss (1 dB) and a good XT level, but the bandwidth of the side-lobes is becoming an issue if the VCSEL's wavelength is imprecise. This problem is alleviated by the flat-top cascaded MZIs, but at the cost of a higher XT (-17.6 dB).

Last and not least, in the case of a 16-channel demultiplexer, as shown in Figure 10 the cascaded MZIs are now 4.6 times bigger than the AWGs. From table V, only the Gaussian devices have an XT below -20 dB (-22.7 dB for the AWG and -24.4 dB for the cascaded MZIs). However, due to the small channel spacing (2 nm), the VCSEL alignment is a critical issue. Indeed, the Gaussian cascaded MZI may have the best XT average but its side-lobes become an even more significant problem than for an 8-channel system if the VCSEL's wavelength is imprecise. The flat-top cascaded MZI is more tolerant to VCSEL misalignment due to its much thinner side-lobes but the average XT is a little higher than the target value (-18.1 dB). The Gaussian AWG offers the second best XT average and the smallest footprint (1.24 mm^2) but the required EBL area is considerable (385000 μm^2) compared to that of the cascaded MZIs (approximately 35000 μm^2 for the Gaussian and flat-top devices). The XT level of the flat-top cascaded MZI can be reduced with additional MZI stages combined with wide and narrow waveguides [27]. Another possibility consists in using a completely different combination of arbitrary coupling coefficients DCs and MMIs as proposed in Ref [25] in the O-band.

V. CONCLUSION

We provided a study of the impact of the number of channels for AWGs and cascaded MZIs on the insertion loss, crosstalk, footprint and fabrication tolerance. We manufactured and demonstrated 4-channel Gaussian AWGs and cascaded MZIs with channel spacing of respectively 7.3 and 7.6 nm. The measurements showed that the Gaussian cascaded MZI provided the best performance in terms of transmission and XT level. The flat-top cascaded MZI is more tolerant to VCSEL misalignment, but at the cost of a much higher XT and would require additional stages to offer lower XT [10], [18]. In addition, the results in Section II show that the cascaded MZIs offer a better manufacturing tolerance and perform better than AWGs at high temperature.

When increasing the number of channels, the AWG, unlike the MZI lattice filter, can still fit in a reasonably small space (1.2 mm^2) and is almost five times smaller than the cascaded MZI in a 16-channel system. However, this is not enough to compensate its eleven times higher EBL writing area. We found that the number of channels has an impact on the insertion loss and XT level for some devices. The Gaussian AWG and cascaded MZI provide similar XT levels, which have a tendency to increase with the number of channels, from -28 dB to close to -23 dB at 4 and 16 channels respectively. However, at 16 channels, the Gaussian MZI requires a much more precise VCSEL wavelength accuracy due to the side-lobes. Therefore, there is a complex tradeoff between size, crosstalk, loss and manufacturing tolerance. We also found that the number of channels has a significant impact on the insertion loss and XT level of the flat-top AWG as they both considerably increase in a 16-channel demultiplexing system. Here, the use of parabolic MMIs is twofold, as it allows a strong reduction of the inter-band flatness, making the device more robust to VCSEL wavelength inaccuracy. However, this is at the cost of high XT and insertion loss. The flat-top cascaded MZI allows a strong reduction of the bandwidth of the sidelobes, but the use of additional stages with a combination of wide and narrow waveguides and broadband directional couplers may be required to reduce the XT level [10], [18], [25], [27], [31], [32]. This would further increase the size of the device, but its lower fabrication complexity compared to that of the AWG might be attractive for 16-channel demultiplexing.

ACKNOWLEDGMENT

This work was funded by European Union's Horizon 2020 research and the Swedish Research Council (2016-06077, iTRAN project). This work was also performed in part at Myfab Chalmers.

REFERENCES

[1] A. Larsson, J. S. Gustavsson, E. Haglund, E. P. Haglund, E. Simpanen, and T. Lengyel, "VCSEL modulation speed: status and prospects," in *Proceedings of SPIE*, San Francisco, California, United States, 2019.

[2] X. Hu, M. Girardi, Z. Ye, P. Muñoz, A. Larsson, and V. Torres-Company, "Si3N4 photonic integration platform at 1 μm for optical interconnect," *Optics express*, vol. 28, no. 9, pp. 13 019–13 031, 2020.

[3] D. Mahgerefteh, C. Thompson, C. Cole, G. Denoyer, T. Nguyen, I. Lyubomirsky, C. Kocot, and J. Tatum, "Techno-economic comparison of silicon photonics and multimode VCSELs," *Journal of Lightwave Technology*, vol. 34, no. 2, pp. 233–242, 2016.

[4] J. A. Tatum, D. Gazula, L. A. Graham, J. K. Guenter, R. H. Johnson, J. King, C. Kocot, G. D. Landry, I. Lyubomirsky, A. N. MacInnes, E. M. Shaw, K. Balemarthy, R. Shubochkin, D. Vaidya, M. Yan, and F. Tang, "VCSEL-based interconnects for current and future data centers," *Journal of Lightwave Technology*, vol. 33, no. 4, pp. 727–732, 2015.

[5] M. Freebody, "Lasers evolve to meet the demands of optical communications," *Photonics spectra*, vol. 46, no. 02, pp. 50–53, 2012.

[6] E. Simpanen, J. Gustavsson, E. Haglund, E. Haglund, A. Larsson, W. Sorin, S. Mathai, and M. Tan, "1060 nm single-mode vertical-cavity surface-emitting laser operating at 50 Gbit/s data rate," *Electronics letters*, vol. 53, no. 13, pp. 869–871, 2017.

[7] A. Larsson, E. Simpanen, J. Gustavsson, E. Haglund, E. Haglund, T. Lengyel, P. Andrekson, W. Sorin, S. Mathai, M. Tan, and S. Bickham, "1060 nm VCSELs for long-reach optical interconnects," *Elsevier Optical Fiber Technology*, vol. 44, pp. 36–42, 2018.

[8] M.-J. Li, "Novel optical fibers for data center applications," in *Proceedings of SPIE*, San Francisco, California, United States, 2016.

[9] M. Jahed, J. S. Gustavsson, and A. Larsson, "VCSEL wavelength setting by intra-cavity phase tuning - numerical analysis and experimental verification," *IEEE Journal of Quantum Electronics*, vol. 57, no. 6, pp. 1–7, 2021.

[10] S. S. Cheung and M. R. T. Tan, "Silicon nitride (Si3N4) (de-)multiplexers for 1-μm CWDM optical interconnects," *Journal of Lightwave Technology*, vol. 38, no. 13, pp. 3404–3413, 2020.

[11] S. Sweeney, A. Phillips, A. Adams, E. O'reilly, and P. Thijs, "The effect of temperature dependent processes on the performance of 1.5-μm compressively strained InGaAs (p) MQW semiconductor diode lasers," *IEEE Photonics Technology Letters*, vol. 10, no. 8, pp. 1076–1078, 1998.

[12] R. Baets, A. Z. Subramanian, S. Clemmen, B. Kuyken, P. Bienstman, N. L. Thomas, G. Roelkens, D. V. Thourhout, P. Helin, and S. Severi, "Silicon photonics: silicon nitride vs silicon-on-insulator," in *Optical Fiber Communications Conference and Exhibition (OFC)*, Anaheim, CA, USA, 2016, pp. 1–3.

[13] T. Akiyama, S. Oda, Y. Nakasha, A. Hayakawa, S. Tanaka, Y. Tanaka, and T. Hoshida, "Casacaded AMZ triplets: a class of demultiplexers having a monitor and control scheme enabling dense WDM on Si nanowaveguide PICs with ultralow crosstalk and high spectral efficiency," *Optics express*, vol. 29, no. 6, pp. 7966–7985, 2021.

[14] D. Dai and J. E. Bowers, "Silicon-based on chip multiplexing technologies and devices for peta-bit optical interconnects," *Nanophotonics de Gruyter*, vol. 3, no. 4-5, pp. 283–311, 2013.

[15] A. A. Bernussi, L. G. de Peralta, V. Gorbounov, J. A. Linn, S. Frisbie, R. Gale, and H. Temkin, "Mirror quality and the performance of reflective arrayed-waveguide grating multiplexers," *Journal of Lightwave Technology*, vol. 22, no. 7, pp. 1828–1832, 2004.

[16] J.-J. He, B. Lamontage, A. Delâge, L. Erickson, M. Davies, and E. S. Koteles, "Monolithic integrated wavelength demultiplexer based on a waveguide rowland circle grating in InGaAsP/InP," *Journal of Lightwave Technology*, vol. 16, no. 4, pp. 631–638, 1998.

[17] F. Horst, W. M. J. Green, S. Assefa, S. M. Shank, Y. A. Vlasov, and B. J. Offrein, "Cascaded Mach-Zehnder wavelength filters in silicon photonics for low loss and flat pass-band WDM (de-)multiplexing," *Optics express*, vol. 21, no. 10, pp. 11 652–11 658, 2013.

[18] H. Xu and Y. Shi, "Flat-top CWDM (de)multiplexer based on MZI with bent directional couplers," *IEEE Photonics Technology Letters*, vol. 30, no. 2, 2018.

[19] P. Pan, J. An, J. Zhang, Y. Wang, H. Wang, L. Wang, X. Yin, Y. Wu, J. Li, Q. Han, and X. Hu, "Flat-top AWG based on InP deep ridge waveguide," *Elsevier Optical Communications*, vol. 255, pp. 376–381, 2015.

[20] M. Girardi, A. Larsson, and V. Torres-Company, "Performance tradeoffs in low-loss Si3N4 waveguides for linear and nonlinear applications," in *European Conference on Integrated Optics*, Milano, Italy, 2022.

[21] J. F. Bauters, M. J. R. Heck, D. John, D. Dai, M.-C. Tien, J. S. Barton, A. Leinse, R. G. Heideman, D. J. Blumenthal, and J. E. Bowers, "Ultra-low-loss high-aspect-ratio Si3N4 waveguides," *Optics express*, vol. 19, no. 4, pp. 3163–3174, 2011.

[22] M. Jahed, J. S. Gustavsson, and A. Larsson, "Precise setting of microcavity resonance wavelength by dry etching," *Journal of Vacuum Science and Technology B*, vol. 37, no. 031217, 2019.

[23] M. S. Hai, A. Leinse, T. Veenstra, and O. Liboiron-Ladouceur, "A thermally tunable 1 x 4 channel wavelength demultiplexer designed on a low-loss Si3N4 waveguide platform," *Photonics*, vol. 2, pp. 1065–1080, 2015.

[24] S. Tao, Q. Huang, L. Zhu, J. Liu, Y. Zhang, Y. Huang, Y. Wang, and J. Xia, "Athermal 4-channel (de-)multiplexer in silicon nitride fabricated at low temperature," vol. 6, no. 7, pp. 686–691, 2018.

[25] S.-H. Jeong, "Silicon-based flat-topped wavelength filter for low crosstalk, high fabrication tolerance and wideband operating range for CWDM applications," *Optical and Quantum Electronics*, vol. 54, no. 605, 2022.

[26] M. Cherchi, F. Sun, M. Kapulainen, M. Harjanne, and T. Aalto, "Flat-top interleavers based on single mmis," in *SPIE OPTO*, San Francisco, California, United States, 2020.

[27] T.-H. Yen and Y.-J. Hung, "Fabrication-tolerant CWDM (de)multiplexer based on cascaded mach–zehnder interferometers on silicon-on-insulator," *Journal of Lightwave Technology*, vol. 39, no. 1, pp. 146 – 153, 2021.

[28] A. Arbabi and L. L. Goddard, "Measurements of the refractive indices and thermo-optic coefficients of Si3N4 and SiOx using microring resonances," *Optics Letters*, vol. 38, no. 19, pp. 3878–3881, 2013.

[29] A. W. Elshaari, I. E. Zadeh, K. D. Jöns, and V. Zwiller, "Thermo-optic characterization of silicon nitride resonators for cryogenic photonic circuits," *IEEE Photonics Journal*, vol. 8, no. 3, 2016.

[30] J. Wang, Z. Sheng, L. Li, A. Pang, A. Wu, W. Li, X. Wang, S. Zou, M. Qi, and F. Gan, "Low-loss and low-crosstalk 8 × 8 silicon nanowire AWG routers fabricated with CMOS technology," *Optics express*, vol. 22, no. 8, pp. 9395–9403, 2014.

[31] D. Mao, Y. Wang, E. El-Fiky, L. Xu, A. Kumar, M. Jacques, A. Samani, O. Carpentier, S. Bernal, M. S. Alam, J. Zhang, M. Zhu, P.-C. Koh, and D. V. Plant, "Adiabatic coupler with design-intended splitting ratio," *Journal of Lightwave Technology*, vol. 37, no. 24, pp. 6147–6155, 2019.

[32] L. Xu, Y. Wang, A. Kumar, E. El-Fiky, D. Mao, H. Tamazin, M. Jacques, Z. Xing, M. G. Saber, and D. V. Plant, "Compact high-performance adiabatic 3-dB coupler enabled by subwavelength grating slot in the silicon-on-insulator platform," *Optics express*, vol. 26, no. 23, pp. 29 873–29 885, 2018.